Dev Cell. Author manuscript; available in PMC 2015 July 01.

Published in final edited form as:
Dev Cell. 2012 April 17; 22(4): 837–848. doi:10.1016/j.devcel.2012.01.006.

GLI3 Constrains Digit Number by Controlling Both Progenitor Proliferation and BMP-Dependent Exit to Chondrogenesis

Javier Lopez-Rios[1], **Dario Speziale**[1,5], **Dimitri Robay**[1,5,6], **Martina Scotti**[3,5], **Marco Osterwalder**[1], **Gretel Nusspaumer**[2], **Antonella Galli**[1,7], **Georg A. Holländer**[2,4], **Marie Kmita**[3], and **Rolf Zeller**[1,*]

[1]Developmental Genetics, Department of Biomedicine, University of Basel, 4058 Basel, Switzerland [2]Department of Biomedicine and Children's Hospital, University of Basel, 4058 Basel, Switzerland [3]Laboratory of Genetics and Development, Institut de Recherches Cliniques de Montréal, Montréal, Québec H2W1R7, Canada [4]Developmental Immunology, Department of Pediatrics, University of Oxford, Oxford OX3 9DU, UK

SUMMARY

Inactivation of *Gli3*, a key component of Hedgehog signaling in vertebrates, results in formation of additional digits (polydactyly) during limb bud development. The analysis of mouse embryos constitutively lacking *Gli3* has revealed the essential GLI3 functions in specifying the anteroposterior (AP) limb axis and digit identities. We conditionally inactivated *Gli3* during mouse hand plate development, which uncoupled the resulting preaxial polydactyly from known GLI3 functions in establishing AP and digit identities. Our analysis revealed that GLI3 directly restricts the expression of regulators of the G_1–S cell-cycle transition such as *Cdk6* and constrains S phase entry of digit progenitors in the anterior hand plate. Furthermore, GLI3 promotes the exit of proliferating progenitors toward BMP-dependent chondrogenic differentiation by spatiotemporally restricting and terminating the expression of the BMP antagonist *Gremlin1*. Thus, *Gli3* is a negative regulator of the proliferative expansion of digit progenitors and acts as a gatekeeper for the exit to chondrogenic differentiation.

INTRODUCTION

Hedgehog signaling is a major regulator of organogenesis in both vertebrate and invertebrate embryos (Jiang and Hui, 2008; Varjosalo et al., 2006). Analysis of Sonic Hedgehog (SHH) signaling has provided insights into how SHH orchestrates vertebrate limb bud development (Chiang et al., 2001; Harfe et al., 2004; Riddle et al., 1993; Zeller et al., 2009). In the

*Correspondence: rolf.zeller@unibas.ch.
[5]These authors contributed equally to this work
[6]Present address: Basilea Pharmaceutica International, 4005 Basel, Switzerland
[7]Present address: Department of Medicine and Genetics & Development, Herbert Irving Comprehensive Cancer Center, Columbia University Medical Center, New York, NY 10032, USA

SUPPLEMENTAL INFORMATION

Supplemental Information includes five figures and Supplemental Experimental Procedures and can be found with this article online at doi:10.1016/j.devcel.2012.01.006.

posterior mesenchyme, SHH is produced by the polarizing region (ZPA) to control anteroposterior (AP) axis specification and proliferative expansion of mesenchymal progenitors together with FGF and Wnt signals (ten Berge et al., 2008; Towers et al., 2008; Zhu et al., 2008). All three types of signals stimulate the expression of *Mycn*, which appears to be a key regulator of limb bud mesenchymal cell proliferation because its inactivation decreases proliferation, resulting in smaller limb skeletal elements and syndactyly (Ota et al., 2007).

SHH is part of a self-regulatory system that interlinks the ZPA with the apical ectodermal ridge (AER) and controls limb bud outgrowth by coordinating BMP, FGF, and SHH signaling with the clearance of retinoic acid from the distal mesenchyme (Probst et al., 2011; Zeller et al., 2009). A key node in this system is the BMP antagonist Gremlin1 (GREM1), which keeps BMP activity low during limb bud outgrowth (Bénazet et al., 2009). This feedback signaling system is self-terminating, as (1) the expanding population of *Shh* descendants is refractory to *Grem1* expression (Scherz et al., 2004), and (2) high AER-FGF signaling inhibits *Grem1* expression in the distal mesenchyme (Verheyden and Sun, 2008). AER-FGF signaling increases during limb bud outgrowth, which eventually inhibits *Grem1* expression. This termination of *Grem1* expression results in a renewed raise of BMP activity (Bénazet et al., 2009; Verheyden and Sun, 2008), which initiates condensation and chondrogenic differentiation of mesenchymal progenitors (Bandyopadhyay et al., 2006; Pizette and Niswander, 2000). In digit primordia, differential BMP signal transduction in the distal phalanx-forming region is likely required to determine the definitive identities (Suzuki et al., 2008; Witte et al., 2010).

In vertebrates, the expression of SHH target genes is regulated by the GLI1-3 transcription factors. In particular, SHH signal transduction at the primary cilia inhibits the proteolytic processing of GLI3 to a transcriptional repressor (GLI3R; Wen et al., 2010). This results in accumulation of GLI1-3 activators in the posterior limb bud, whereas GLI3R is the predominant GLI isoform in the anterior mesenchyme (Ahn and Joyner, 2004; Wang et al., 2000). A genome-wide screen for *cis*-regulatory regions bound by an epitope-tagged GLI3R transgene in mouse limb buds has identified ~200 candidate transcriptional targets, among them *Grem1* and the cell-cycle regulator *Cdk6* (Vokes et al., 2008). Loss-of-function mutations in the mouse *Gli3* gene cause preaxial and central polydactylies with soft tissue fusions (polysyndactyly), a prominent feature shared with human congenital malformations caused by mutations in *GLI3* (Biesecker, 2006). Analysis of the *extra-toes* (*Xt*) loss-of-function mutation in mice has been instrumental to uncover essential requirements of *Gli3* (Hui and Joyner, 1993; Schimmang et al., 1992). In limb buds, *Gli3* is expressed from early stages onward and interacts with the *Hand2* and *5′ Hoxd* transcription factors to polarize the nascent mesenchyme and restrict *Shh* activation to the posterior mesenchyme (Galli et al., 2010; te Welscher et al., 2002a; Zakany et al., 2007). In *Gli3*-deficient mouse limb buds, posterior genes are expressed ectopically, whereas anterior genes are downregulated (Büscher et al., 1997; Hill et al., 2009; Litingtung et al., 2002; McGlinn et al., 2005; te Welscher et al., 2002b; Zúñiga and Zeller, 1999). Hence, *Gli3* participates in setting up the AP limb bud axis, but the extent to which posterior identity is retained in *Gli3*-deficient limb buds remained unclear (Galli et al., 2010; Hill et al., 2009). Limb buds deficient for both *Gli3* and *Hand2* lack AP polarity and are highly polydactylous (Galli et al., 2010), whereas

the polydactyly of mouse limbs lacking both *Gli3* and *Shh* is indistinguishable from *Gli3* mutants (Litingtung et al., 2002; te Welscher et al., 2002b). Molecular analysis indicated that one major function of SHH is to counteract GLI3R-mediated repression of distal limb and digit development. Furthermore, the massive apoptosis observed in *Shh*-deficient limb buds has been linked to increased GLI3R levels and aberrantly high BMP activity (Bastida et al., 2004). Indeed, the incompletely penetrant anterior digit duplications in heterozygous Xt^J ($Gli3^{XtJ/+}$) mice are enhanced by additional heterozygosity for a *Bmp4* loss-of function allele (Dunn et al., 1997). Similarly, transgene-mediated ectopic *Hoxd12* expression enhances the digit polydactyly because GLI3R forms a transcriptional activator complex with HOXD12 that promotes the formation of additional digits (Chen et al., 2004). The digit polydactyly of *Gli3*-deficient limbs is also enhanced by deletion of *5′ HoxD* genes, which results in an anterior gain of *Hoxd9* and *Hoxd10* expression (Sheth et al., 2007).

We generated a conditional loss-of-function *Gli3* allele and inactivated *Gli3* specifically in the developing hand plate (autopod) of mouse limb buds. This allowed us to uncover the dual mechanism by which GLI3 controls digit morphogenesis and restrains the autopod to five digits (pentadactyly). In the anterior mesenchyme, GLI3 acts as a gatekeeper of the G_1–S transition by regulating the expression of cell-cycle genes and S phase entry. In addition, GLI3 restricts and terminates *Grem1* expression in the anterior autopod in a spatiotemporally controlled manner, which promotes the BMP-dependent exit of progenitors from proliferation to chondrogenic differentiation. Disruption of this dual role underlies the resulting preaxial polydactylies because progenitors continue to proliferate, and the onset of chondrogenic differentiation is delayed in the absence of *Gli3*. This study shows how GLI3 tightly controls the kinetics and length of proliferative expansion and constrains the developing limb bud to pentadactyly.

RESULTS

Constitutive Loss of *Gli3* Alters the Anterior but Not Posterior Autopod

To assess the extent of posterior development in *Gli3*-deficient forelimb buds, mesenchymal progenitors were marked by activation of a *LacZ* reporter gene in *Shh*-expressing cells and their descendants (Harfe et al., 2004). Despite the lack of *Gli3* and anterior ectopic SHH signaling (see Figure S1 available online), the descendants contributed equally to the posterior-most digits d5 and d4, and no ectopic anterior spot of LacZ-positive cells was detected in *Gli3*-deficient limb buds (Figure 1A; see also Harfe et al., 2004). The central and posterior digits 3–5 were readily identified by their morphology and extent of metacarpal ossification in *Gli3*-deficient limbs (Figure 1B). Several additional anterior digits formed, but the anterior-most digit 1 was lost in *Gli3*-deficient limbs (Figure 1B). These results showed that posterior cell fates were maintained and that the polydactyly arose from the anterior and central autopod in mutant limb buds. Real-time quantitative PCR (qPCR) and RNA in situ hybridization showed that the expression of SHH targets such as the transcriptional regulators *5′ Hoxd*, *Hand2*, and *Gli1* was increased in the anterior mesenchyme (Figure S1).

Conditional Inactivation of *Gli3* in the Developing Autopod

To study the spatiotemporal requirements of *Gli3*, we generated a conditional loss-of-function $Gli3^{f}$ allele (Figures 1C and S1). Cre-mediated recombination of the $Gli3^{f}$ allele resulted in a deletion that encompassed the DNA binding and transactivation domains as in the constitutive $Gli3^{XtJ}$ null allele, but only 15 kb instead of 51 kb was deleted (Maynard et al., 2002). An additional *Gli3* null allele ($Gli3^{\Delta}$) was generated by germline recombination of the $Gli3^{f}$ allele. Genetic complementation with the $Gli3^{XtJ}$ allele showed that this $Gli3^{\Delta}$ allele reproduces the pleiotropic range of *Gli3* loss-of function phenotypes (Figure S1; data not shown). Therefore, both *Gli3* null alleles were used interchangeably and are referred to as $Gli3^{\Delta}$ alleles. In addition, *Prx1*-Cre-mediated inactivation of *Gli3* from early limb bud stages onward ($Gli3^{\Delta/\Delta c}$; *P1*-Cre) caused an anterior polydactyly indistinguishable from $Gli3^{XtJ/XtJ}$ limbs (Figure 1D; compare to Figure 1B).

We inactivated the $Gli3^{f}$ allele specifically during autopod development in forelimb buds ($Gli3^{\Delta c}$ allele) using a mouse strain expressing the Cre-recombinase under control of the *Hoxa13* locus ($Hoxa13^{Cre/+}$, Figure 1E; Scotti and Kmita, 2012). At embryonic day (E) 10.5, the *Gli3* transcript distribution was not affected, whereas by ~E11.75, *Gli3* transcripts had cleared from the distal autopod of $Gli3^{\Delta/\Delta c}$ forelimb buds (lower panels, Figure 1E). Immunoblotting showed that both the full-length GLI3 (GLI3FL) and GLI3R protein isoforms were no longer detectable in the distal part of the $Gli3^{\Delta/\Delta c}$ autopod, whereas levels in the proximal part remained similar to $Gli3^{\Delta/+}$ controls (Figures 1F and 1G). To exclude phenotypic and/or molecular variations due to heterozygosity for *Hoxa13* in $Gli3^{\Delta/\Delta c}$ forelimb buds, all other embryos (wild-type, $Gli3^{\Delta/+}$, and $Gli3^{\Delta/\Delta}$) analyzed also carried one $Hoxa13^{Cre/+}$ allele (Figures 2, 3, 4, 5, 6, and 7).

Inactivation of *Gli3* by *Hoxa13*-Cre Uncouples Preaxial Polydactyly from AP Axis Specification

Analysis of $Gli3^{\Delta/\Delta c}$ forelimbs at E16.5 revealed a distinct preaxial polydactyly (n = 42/42, Figure 2A). In general, the duplications affected digits 1 and 2 (asterisks in Figure 2A), and anterior character was retained in contrast to $Gli3^{\Delta/\Delta}$ forelimbs. All $Gli3^{\Delta/+}$, $Hoxa13^{Cre/+}$ forelimbs were phenotypically normal (n = 10/16) or displayed only minor dysmorphologies (n = 6/16; data not shown). Anterior ectopic or expanded mesenchymal expression of *Gli1*, *Hoxd12*, *Hoxd13*, and AER-*Fgf8* hallmarks the *Gli3* loss-of-function phenotype (panels $Gli3^{\Delta/\Delta}$, Figures 2B–2E; Büscher et al., 1997; Zúñiga and Zeller, 1999), but none of these genes were significantly altered in $Gli3^{\Delta/\Delta c}$ forelimb buds (panels $Gli3^{\Delta/\Delta c}$, Figures 2B–2E). Rarely, very small ectopic patches of *5′ Hoxd* transcripts (*Hoxd13*, n = 1/9; *Hoxd12*, n = 2/6) were detected in $Gli3^{\Delta/\Delta c}$ forelimb buds (data not shown), but the anterior expression boundaries were otherwise maintained (panels $Gli3^{\Delta/\Delta c}$, Figures 2B–2E). This indicated that anterior and posterior identities were retained in $Gli3^{\Delta/\Delta c}$ forelimb buds. At E11.75, the size of $Gli3^{\Delta/\Delta c}$ hand plates was still normal in contrast to the enlarged autopod primordia in $Gli3^{\Delta/\Delta}$ forelimb buds (Figures 2B–2E). Morphometric analysis revealed that only by E12.5, both $Gli3^{\Delta/\Delta c}$ (+38% ± 14%) and $Gli3^{\Delta/\Delta}$ hand plates (+46% ± 12%) were enlarged in comparison to wild-type controls (Figure S2; data not shown). Although the anterior-most digit in $Gli3^{\Delta/\Delta c}$ forelimbs was clearly dysmorphic, the analysis of molecular markers revealed the normal anterior digit 1 expression domains (Figure S2). Therefore, inactivation

of *Gli3* during autopod development uncoupled the preaxial polydactyly from alterations of the AP axis and showed that GLI3R is required to restrain the autopod to pentadactyly long after SHH-dependent specification of AP identities (Zhu et al., 2008).

Shared Molecular Signatures of the Two *Gli3*-Deficient Polydactylies

The transcriptomes of both types of *Gli3*-deficient anterior autopods were compared to wild-types at E11.75 to identify shared molecular alterations. The transcriptome of three independent anterior autopod samples per genotype was analyzed (Figure 3A). Hierarchical clustering revealed that the transcriptomes of $Gli3^{\Delta/\Delta c}$ and $Gli3^{\Delta/\Delta}$ anterior autopods were more similar to each other than wild-type and $Gli3^{\Delta/+}$ control samples (all carrying the $Hoxa13^{Cre/+}$ allele; Figure 3B). These microarray data sets were biologically significant because all known anterior alterations in $Gli3^{XtJ/XtJ}$ limb buds (Figure S1; McGlinn et al., 2005) and the normal expression of anterior genes in $Gli3^{\Delta/\Delta c}$ forelimb buds were detected (Figures 2 and S2). Ingenuity Pathway Analysis and validation of the detected alterations by qPCR and RNA in situ hybridization revealed striking transcriptional changes. In particular, the core module that regulates the G_1–S transition of the cell cycle was specifically altered in both $Gli3^{\Delta/\Delta c}$ and $Gli3^{\Delta/\Delta}$ anterior autopods (indicated by broken line, Figure 3C; Neganova and Lako, 2008), whereas *Mycn* and most other cell-cycle regulators were not consistently changed (Figures 3C and S3). The significant upregulation and anterior expansion of the cyclin/kinase pair *Cdk6* (~1.9-fold) and *Ccnd1* (~1.3-fold) in the anterior hand plate of both types of *Gli3*-deficient forelimb buds were confirmed by qPCR and RNA in situ hybridization analysis (Figures 3D and 3E). The expression of *Cdkn2c*, encoding a CDK4/6 inhibitor (Sherr and Roberts, 1995), was reduced ~0.65-fold (Figure 3D). In summary, this transcriptome analysis revealed that the G_1–S transition of the cell cycle was specifically altered in the anterior of *Gli3*-deficient autopods.

Altered Cell-Cycle Kinetics of Digit Progenitors in the Anterior Autopod

To directly assess the relevance of these transcriptional changes with respect to the cell cycle, mouse embryos were labeled with BrdU for 1 hr, and anterior and posterior autopods were dissected from age-matched $Gli3^{\Delta/\Delta}$ (n = 5 at E11.75; ~50 somites) and control littermates (n = 7). Dead cells (≤10% in all genotypes), erythrocytes, and debris were excluded using the appropriate gates, and intact single cells were analyzed by flow cytometry (Figures 4A and 4B) to determine the fractions of cells in three distinct phases of the cell cycle (G_0–G_1, S, and G_2–M; Figure 4A). Cells in S phase contained high levels of BrdU and DNA, whereas cells in the G_0–G_1 (low DNA content) and G_2–M (high DNA content) phases had incorporated little or no BrdU (Figure 4A). No significant changes were detected between anterior and posterior parts of control autopods or with posterior parts of $Gli3^{\Delta/\Delta}$ mutant autopods (Figures 4A and 4B). This contrasted with the anterior part of *Gli3*-deficient autopods because the fraction of cells in S phase was increased by ~25% ($p \leq 0.01$; Figures 4A and 4B). Concurrently, the fraction of cells in the G_0–G_1 transition of the cell cycle was decreased by ~17% ($p \leq 0.01$; Figure 4B). These alterations revealed that cell-cycle entry was significantly enhanced in the anterior part of *Gli3*-deficient autopods (Figures 4A and 4B), in agreement with the specific transcriptional changes of regulators of the G_1–S transition (Figures 3C–3E).

A previous genome-wide search for *cis*-regulatory sequences interacting with an exogenous epitope-tagged GLI3R protein in mouse embryos had identified *Cdk6* as a potential transcriptional target of GLI3 (Vokes et al., 2008). To gain further insight into the possible direct regulation of *Cdk6* by GLI3, specific antibodies (Wen et al., 2010) were used for comparative chromatin immunoprecipitation (ChIP) analysis of wild-type and $Gli3^{\Delta/\Delta}$ forelimb bud extracts (Figure 4C). This analysis established that endogenous GLI3 proteins interact specifically with this genomic region located just upstream of the *Cdk6*-coding region in wild-type limb buds (~4-fold enrichment), whereas no interaction was detected in mutant limb buds (Figure 4C). The functional importance of this regulatory interaction was assessed by analyzing mouse forelimb buds lacking both *Gli3* and *Cdk6* (Figures 4D and 4E; Malumbres et al., 2004). Although up to seven digit rays formed in $Gli3^{\Delta/\Delta}$ forelimb buds (n = 6/8), only six with duplicated distal-most phalanges formed in the majority of all $Gli3^{\Delta/\Delta}$, $Cdk6^{\Delta/\Delta}$ forelimbs (n = 12/17, Figure 4D). In contrast, the less-pronounced preaxial polydactyly in $Gli3^{\Delta/\Delta c}$ forelimbs was not affected by additional inactivation of *Cdk6* (n = 6/6, Figure 4E). This genetic analysis established the sensitivity of the $Gli3^{\Delta/\Delta}$, but not $Gli3^{\Delta/\Delta c}$, polydactyly to *Cdk6* inactivation. In agreement, FGF signaling, which stimulates proliferation, was increased in the anterior of $Gli3^{\Delta/\Delta}$ but not $Gli3^{\Delta/\Delta c}$ forelimb buds (Figures 2E and S3), whereas Wnt signaling was not altered (data not shown).

Decreased BMP Activity in the Anterior of *Gli3*-Deficient Limb Buds

Ingenuity Pathway Analysis also revealed major alterations of BMP signaling in anterior *Gli3*-deficient autopods (Figure S4). In particular, the expression of several targets of the BMP pathway such as *Msx2*, *Id1*, and *Id3* was reduced ~2-fold in *Gli3*-deficient anterior autopods (Figures 5A, 5C, and S4). This reduction in BMP signal transduction was paralleled by a ≥2-fold increase in *Grem1* transcripts, whereas the expression of *Bmp* ligands was not consistently altered (Figures 5B, 5C, and S4). In $Gli3^{\Delta/\Delta}$ limb buds, *Grem1* expression is expanded anteriorly from the onset of limb bud development onward (te Welscher et al., 2002a), whereas in $Gli3^{\Delta/\Delta c}$ forelimbs its anterior expansion occurred much later and concurrent with *Hoxa13*-Cre-mediated inactivation of *Gli3* (Figure 5B, compare to lower panels in Figure 1E). Furthermore, *Grem1* transcripts persisted in the anterior of both types of *Gli3*-deficient forelimb buds, whereas in wild-types transcripts became undetectable in the presumptive digit primordia by E12.5 (lower panels, Figure 5B). ChIP analysis established that the endogenous GLI3 proteins interacted with a known *cis*-regulatory region within the *Grem1* genomic landscape (~6- to 8-fold enrichment, Figure 5D; Vokes et al., 2008).

Gli3 Inactivation Delays the BMP-Dependent Exit of Proliferating Digit Progenitors to Chondrogenesis in the Anterior Mesenchyme

Because BMP signaling is required to initiate mesenchymal condensations and chondrogenic differentiation (Pizette and Niswander, 2000; Yoon et al., 2005), we analyzed the distribution of Sox9, which marks the precartilaginous condensations of the forming skeletal primordia (Ng et al., 1997). In wild-type forelimb buds, five distinct Sox9-positive digit primordia were apparent by E12.5 (n = 3/3, left panel, Figure 6A). In contrast, only the posterior condensations were apparent in both types of *Gli3*-deficient autopods (n = 3/3, Figure 6A). To correlate Sox9-positive with proliferating cells, the distribution of Ki67,

which marks all proliferating cells (Gerdes et al., 1983), was assessed on parallel sections (Figures 6A and 6B). In wild-types, few Ki67-positive cells were detected in the Sox9-positive condensations of the digit primordia, whereas the surrounding mesenchyme continued to proliferate (left panels, Figure 6B). In *Gli3*$^{\Delta/\Delta}$ autopods, most cells in the anterior mesenchyme remained Ki67 positive (middle panels, Figure 6B), and in *Gli3*$^{\Delta/\Delta c}$ autopods, Ki67 persisted throughout the distal-most mesenchyme (right panels, Figure 6B). *Noggin* and *Col2a1*, two molecular markers of chondrogenic differentiation, delineated all digit primordia in wild-types, but only the posterior ones in *Gli3*-deficient autopods (Figure 6C; McGlinn et al., 2005). In *Gli3*-deficient forelimb buds, the anterior-most condensation appeared reduced and forked, and the small primordia for digit 1 was absent (Figure 6C). Taken together, this analysis established that in *Gli3*-deficient forelimb buds, the anterior mesenchymal progenitors continued to proliferate and failed to initiate chondrogenic differentiation at the right time. To determine if this delayed exit toward chondrogenic differentiation was indeed caused by an excess of GREM1-mediated BMP antagonism, beads loaded with 0.5 mg/ml BMP4 were implanted into the anterior of *Gli3*-deficient forelimb buds (Figure 6D). These grafts induced strong expression of both *Noggin* and *Col2a1* in the anterior mutant mesenchyme (right panels, Figure 6D), but in contrast to grafts into younger limb buds (see e.g., Bastida et al., 2004), cellular apoptosis was not increased (data not shown). Hence, a causal link between increased GREM1, aberrantly low BMP activity and delayed chondrogenic differentiation was established. In particular, *Grem1* expression in the anterior mesenchyme terminated around E13.0, which correlated well with the delay in differentiation of anterior digits in *Gli3*-deficient forelimb buds (data not shown).

Because complete inactivation of *Grem1* alters limb bud development from early stages onward in the context of the *Gli3* deficiency (Zúñiga and Zeller, 1999), the phenotypic consequences of genetically reducing *Grem1* in *Gli3*$^{\Delta/\Delta}$ and *Gli3*$^{\Delta/\Delta c}$ forelimbs were determined (Figures 7A and 7B). Although *Gli3*$^{\Delta/\Delta}$, *Grem1*$^{\Delta/+}$ forelimb buds were identical to *Gli3*$^{\Delta/\Delta}$ forelimb buds (Figure 7A), the preaxial polydactyly of *Gli3*$^{\Delta/\Delta c}$ forelimbs (six to seven digit rays, n = 12/12) was reduced to pentadactyly in most cases in *Gli3*$^{\Delta/\Delta c}$, *Grem1*$^{\Delta/+}$ forelimbs (Figure 7B). In particular, distinct *Col2a1*-positive condensations were visible in the positions normally giving rise to digits 2 and 1 in *Gli3*$^{\Delta/\Delta c}$, *Grem1*$^{\Delta/+}$ forelimb buds (upper right panel, Figure 7B, compare to wild-type in Figure 7A). Although an apparently normal digit 2 formed, duplicated distal phalanges persisted on the most-anterior digit in *Gli3*$^{\Delta/\Delta c}$, *Grem1*$^{\Delta/+}$ forelimbs (n = 11/17, lower right panel, Figure 7B). This analysis revealed the differential sensitivity of *Gli3*$^{\Delta/\Delta}$ and *Gli3*$^{\Delta/\Delta c}$ polydactylies to the *Grem1* gene dosage, which is likely linked to the fact that *Grem1* is anteriorly expanded from the earliest stages onward in *Gli3*$^{\Delta/\Delta}$ forelimb buds (te Welscher et al., 2002a), whereas it expands only late during autopod formation in *Gli3*$^{\Delta/\Delta c}$ forelimb buds (Figure 5B).

The genetic interaction of *Gli3* with *Bmp4* and effects on polydactyly were first analyzed in *trans*-heterozygous mouse embryos due to the early lethality of *Bmp4*-deficient mouse embryos (Dunn et al., 1997; see also Figure S5). Therefore, we used *Hoxa13*-Cre to inactivate *Bmp4* (Liu et al., 2004) in a conditional manner during autopod development. Such conditional inactivation of *Bmp4* (*Bmp4*$^{\Delta/\Delta c}$) did not alter the anterior autopod likely due to redundancy among *Bmp* ligands (Bandyopadhyay et al., 2006), but a postaxial

condensation formed in some forelimbs (asterisks, Figure S5, and Figures 7C and 7D). In contrast, inactivation of *Bmp4* in the context of heterozygosity for *Gli3* significantly enhanced the preaxial polydactyly (Figure 7C). Although $Gli3^{\Delta/+}$ forelimbs were pentadactylous, the preaxial polydactyly in $Gli3^{\Delta/+}$, $Bmp4^{\Delta/\Delta c}$ forelimbs was increased to the maximal extent seen in $Gli3^{\Delta/\Delta c}$ forelimbs (n = 10/12, Figure 7C, compare to left panels in Figure 7B). The elongated *Col2a1*-positive condensation that normally forms digit 2 was reduced to a forked rudiment in $Gli3^{\Delta/+}$, $Bmp4^{\Delta/\Delta c}$ forelimb buds (asterisks, Figure 7C). Furthermore, the small anterior condensation giving rise to digit 1 (black arrowhead, Figure 7C) was absent in $Gli3^{\Delta/+}$, $Bmp4^{\Delta/\Delta c}$ forelimb buds (upper right panel, Figure 7C). These results pointed to reduced and/or delayed initiation of chondrogenic differentiation. This polydactylous phenotype was not further enhanced by complete inactivation of both *Gli3* and *Bmp4* (n = 14/14, Figure 7D). Overall, these results corroborate the proposal that aberrantly low BMP activity delays chondrogenic differentiation and contributes to the preaxial polydactylies in *Gli3*-deficient forelimbs.

DISCUSSION

First, we show that constitutive loss of *Gli3* specifically alters the anterior of the developing limb bud, which indicates that the resulting preaxial polydactyly is predominantly caused by disrupting the GLI3R isoform. In fact, it has been recently shown that GLI3R also mediates all essential *Gli3* functions during cortical neurogenesis in mouse embryos (Wang et al., 2011). Second, we establish that conditional inactivation of *Gli3* in the developing autopod uncouples the preaxial polydactylies from the early GLI3 functions in establishment of AP identities (Galli et al., 2010; te Welscher et al., 2002a; Zakany et al., 2007). Therefore, the preaxial polydactyly observed in $Gli3^{\Delta/\Delta c}$ forelimbs must be caused by alterations that occur long after the functions of *Gli3* in setting up the AP limb bud axis and the early specification of digit identities by SHH signaling (Zhu et al., 2008). In this context, GLI3R might be required only early and transiently to restrict the expression of posterior genes (Büscher et al., 1997; Zúñiga and Zeller, 1999).

Most importantly, our study reveals the two distinct regulatory steps by which *Gli3* limits the proliferative expansion of the anterior limb bud mesenchyme and ascertains pentadactyly (Figure 7E). Initially, GLI3 acts as a negative modulator of the G_1–S transition, most probably by directly regulating *Cdk6* transcription. These alterations of the G_1–S transition likely result in faster cycling rather than an increase in proliferating cells because the mitotic index was not altered (M.O. and J.L.-R., unpublished data). Subsequently, GLI3 limits the proliferative expansion of mesenchymal progenitors by restricting and ultimately terminating *Grem1* expression in a spatiotemporally controlled manner in the anterior autopod (Figure 7E). The resulting increase in BMP activity promotes the exit of undifferentiated proliferating progenitors toward chondrogenesis. Therefore, GLI3 fulfills a dual role in constraining proliferation of mesenchymal progenitors by regulating both cell-cycle entry and exit to chondrogenic differentiation. In support of a causal link between these two functions, it has been shown that *Cdk6* overexpression promotes proliferation and interferes with BMP2-induced osteoblast differentiation (Grossel et al., 1999; Ogasawara et al., 2004). Furthermore, these dual GLI3 functions are likely of general relevance because *Gli3* is required together with *Plzf* to initiate chondrogenic differentiation of stylopod and

zeugopodal primordia in hindlimbs (Barna et al., 2005). Moreover, *Gli3* has been shown to balance proliferation with neural differentiation during central nervous system development (Blaess et al., 2008; Wang et al., 2011).

The gene networks regulating limb bud outgrowth and termination of the SHH-dependent signaling system that originates from the posterior autopod have been studied extensively (Figure 7E). The core module of this signaling system is the SHH/GREM1/AER-FGF feedback loop that keeps BMP activity low and promotes coordinated outgrowth of the limb bud (reviewed by Zeller et al., 2009). Its termination results in a renewed increase in BMP activity (Bénazet et al., 2009), which likely promotes mesenchymal condensation and chondrogenic differentiation similar to what the present study establishes for the anterior autopod (Figure 7E). Indeed, genetic inactivation of both *Bmp4* and *Bmp2* interferes with formation of posterior digit primordia (Bandyopadhyay et al., 2006). Taken together, these studies indicate that BMP activity is low during the proliferative expansion of digit progenitors, but high levels are required for exit to chondrogenic differentiation (this study; Bandyopadhyay et al., 2006). Conversely, high BMP levels induce mesenchymal cell death during limb bud outgrowth and patterning (see e.g., Bastida et al., 2004), which in agreement with the present study indicates that proliferating progenitors depend on low BMP activity.

Genetic analysis revealed the differential sensitivity of the two types of *Gli3*-deficiencies to *Cdk6* inactivation and *Grem1* gene dosage. The autopod of $Gli3^{\Delta/\Delta}$ forelimbs was enlarged and the G_1–S transition likely altered from early stages onward, which would render the resulting preaxial polydactyly more sensitive to *Cdk6* inactivation. In contrast, the $Gli3^{\Delta/\Delta}$ polydactyly was not sensitive to heterozygosity for *Grem1*, which may again be a consequence of the early enlargement of the anterior autopod. This occurs during the period of robust and self-regulatory feedback signaling, which will rapidly compensate variations in BMP activity by adjusting *Grem1* expression (Nissim et al., 2006; Bénazet et al., 2009). In contrast, the anterior autopod of $Gli3^{\Delta/\Delta c}$ forelimb buds was only enlarged as feedback signaling terminated, which should render the system susceptible to aberrant *Grem1* expression. This was indeed evidenced by the fact that the preaxial polydactylies in $Gli3^{\Delta/\Delta c}$ forelimbs are sensitive to the *Grem1* gene dose. Therefore, the delayed exit from proliferation to BMP-dependent chondrogenic differentiation due to increased GREM1 activity is likely to contribute proportionally more to the enlargement of the anterior autopod in $Gli3^{\Delta/\Delta c}$ than in $Gli3^{\Delta/\Delta}$ forelimb buds.

In light of the present study, alterations affecting cell-cycle entry and exit to chondrogenic differentiation, rather than bona fide patterning defects, could underlie the congenital malformations observed in patients with Greig's cephalopolysyndactyly and Pallister-Hall syndrome, which are caused by scattered point mutations and deletions in the human *GLI3* gene (reviewed by Biesecker, 2006). The highly variable limb polydactylies in these patients could be a consequence of variations affecting the duration of proliferative expansion of digit progenitors. In fact, Alberch and Gale (1983), using colchicine to inhibit proliferation in amphibian limb buds, realized that local changes in cell proliferation affected the number and identities of digits. They concluded that the number of digits correlated well with the final size of the autopod field, i.e., the extent to which the progenitors expanded. In

agreement, the constitutive loss of *Gli3* causes a more severe preaxial polydactyly than later inactivation during autopod development. Therefore, the dual functions of GLI3 in restricting S phase entry and promoting exit to chondrogenic differentiation are an essential part of the morphoregulatory systems (Figure 7E) that initiate and terminate the rather homogeneous proliferative expansion of limb bud mesenchymal progenitors (Boehm et al., 2010; Gros et al., 2010) and constrain the autopod to pentadactyly.

EXPERIMENTAL PROCEDURES

Mouse Strains and Embryos

Studies with mice were performed in strict accordance with Swiss law and 3R principles. The $Gli3^{XtJ}$ allele was maintained in a NMRI background. The $Gli3^{f}$, $Gli3^{\Delta}$ alleles and *Hoxa13-Cre* alleles were maintained in a mixed 129SvJ/C57BL/6J background. $R26R^{LacZ/+}$, $Shh^{Cre/+}$, *Prx1-Cre*, *Cdk6*, *Grem1*, *Bmp4* null, and *Bmp4* conditional alleles were maintained in a C57BL/6J background. For all studies, wild-type and mutant embryos (age matched, ±1 somite) of the same genetic background were used to exclude phenotypic variation. This analysis focused on forelimbs because *Hoxa13*-Cre is active earlier in hindlimb buds resulting in a *Gli3* null phenotype.

Immunofluorescence and Immunoblot Analysis

Limb buds were fixed overnight in 4% paraformaldehyde at 4˜C, and Sox9 and Ki67 protein were detected on 7 μm serial paraffin sections. Primary antibodies against Sox9 (1:500) and Ki67 (1:200; Millipore) were detected using goat anti-rabbit conjugated to Alexa Fluor 594 (1:500; Invitrogen). Nuclei were counterstained with Hoechst-33258. For immunoblot analysis, forelimb bud pairs were dissected at E11.75 (~52 somites), and 10 μg protein was separated on 6% SDS-PAGE gels, followed by transfer to PVDF membranes (Millipore). GLI3 proteins were detected by chemiluminescence using monoclonal anti-GLI3 antibodies (clone 6F5, 5 μg/ml; Wen et al., 2010).

Microarray Analysis

Total RNA was isolated from the anterior hand plates of forelimb bud pairs of three sex- and somite-matched embryos per genotype. Probes for the independent triplicates were labeled and hybridized to GeneChip Mouse Gene 1.0 ST Arrays (see Probst et al., 2011). Data were analyzed using the Partek Genomic Suite 6.5 software and Ingenuity Pathway Analysis software. The correlation coefficients (r) of biological triplicates of a particular genotype ranged from 0.994 to 0.998. To identify differentially expressed genes, two-way ANOVA analysis was used. The microarray data files are available via MIAMExpress (accession number E-MEXP-3495).

Quantitation of Transcript Levels by Real-Time PCR

The anterior halves of hand plates at E11.75 (~52 somites) were dissected, total RNAs were extracted, and cDNA was synthesized and analyzed by qPCR as described (Bénazet et al., 2009; for primers see Supplemental Experimental Procedures). Relative transcript levels were normalized to the expression of two housekeeping genes, *Rpl19* and *Hprt1*. The expression levels of mutant samples were calculated in relation to wild-type controls

(average set to 100%). All results (mean ± SD) are based on analysis of seven or eight samples per genotype. The significance of all differences was assessed using the two-tailed, nonparametric Mann-Whitney U test.

Flow Cytometric Analysis

Pregnant females were injected intraperitoneally with 2 mg of BrdU 1 hr before sacrifice. Forelimb autopod pairs of individual embryos (E11.75, ~50 somites) were dissected in ice-cold IMDM (Invitrogen) supplemented with 10% FCS (Hyclone) into anterior and posterior halves. Samples were dissociated into single cells using 1 mg/ml collagenase D and 50 μg/ml DNase I in 1× HBSS (Roche). Subsequently, cells were filtered through a 70 μM mesh and decorated with FITC-conjugated anti-BrdU antibodies and 7-AAD (to determine DNA content; BD Bioscience). Samples were cooled on ice during the entire procedure. Flow cytometric analysis was done using a FACScalibur System (BD Biosciences), and primary data were processed using FlowJo software (Tree Star). Initial analysis of DAPI uptake into apoptotic cells established that this dissociation caused less than 10% cell death. In particular, no differences in cell survival were apparent among the different genotypes. Forward and side scatter gates were set to exclude erythrocytes, cell debris, and dead cells. No genotype-specific differences in size or complexity were detected. The significance of all differences was verified by two-tailed, nonparametric Mann-Whitney U test.

Manipulation and Culture of Mouse Limb Buds

Mouse forelimb buds were cultured as described (Probst et al., 2011). Heparin beads were loaded with recombinant BMP4 (0.5 mg/ml in PBS; R&D Systems) and implanted into the anterior autopod of embryos at E12.0 (~56 somites). This BMP4 concentration was used because it neither stimulates *Grem1* expression (Nissim et al., 2006) nor causes significant cell death. Individual forelimb buds were cultured for 12–14 hr, fixed, and analyzed by RNA in situ hybridization. Contralateral limbs with no beads or PBS-soaked beads served as controls.

Supplementary Material

Refer to Web version on PubMed Central for supplementary material.

Acknowledgments

The authors are grateful to D. Klewe-Nebenius and C. Klasen (EMBL) for generating chimeric mice and A. Offinger and her staff for excellent animal care. S. Scales (Genentech) provided the GLI3 antibodies, F. Imhof and A. Hermann participated in aspects of this study as part of their master research projects, and E. Uenal performed the OPT analysis and volumetric measurements. P. Demougin from the University of Basel Lifesciences Training Facility performed the microarray hybridization and primary analysis. We thank J.D. Bénazet, A. Zuniga, and group members for critical input on the manuscript. J.L.-R. received an EMBO long-term and EU Marie Curie postdoctoral fellowship. This research was supported by grants of the Swiss National Science Foundation (grants 31003A_130803 to R.Z. and 310000_122558 to G.A.H.), an EU reintegration grant (PERG-GA-2009-246576 to J.L.-R.), a Canadian Institute of Health Research grant (CIHR-82880 to M.K.), and the University of Basel.

References

Ahn S, Joyner AL. Dynamic changes in the response of cells to positive hedgehog signaling during mouse limb patterning. Cell. 2004; 118:505–516. [PubMed: 15315762]

Alberch P, Gale EA. Size dependence during the development of the amphibian foot. Colchicine-induced digital loss and reduction. J Embryol Exp Morphol. 1983; 76:177–197. [PubMed: 6631320]

Bandyopadhyay A, Tsuji K, Cox K, Harfe BD, Rosen V, Tabin CJ. Genetic analysis of the roles of BMP2, BMP4, and BMP7 in limb patterning and skeletogenesis. PLoS Genet. 2006; 2:e216. [PubMed: 17194222]

Barna M, Pandolfi PP, Niswander L. Gli3 and Plzf cooperate in proximal limb patterning at early stages of limb development. Nature. 2005; 436:277–281. [PubMed: 16015334]

Bastida MF, Delgado MD, Wang B, Fallon JF, Fernandez-Teran M, Ros MA. Levels of Gli3 repressor correlate with Bmp4 expression and apoptosis during limb development. Dev Dyn. 2004; 231:148–160. [PubMed: 15305295]

Bénazet JD, Bischofberger M, Tiecke E, Gonçalves A, Martin JF, Zuniga A, Naef F, Zeller R. A self-regulatory system of interlinked signaling feedback loops controls mouse limb patterning. Science. 2009; 323:1050–1053. [PubMed: 19229034]

Biesecker LG. What you can learn from one gene: GLI3. J Med Genet. 2006; 43:465–469. [PubMed: 16740916]

Blaess S, Stephen D, Joyner AL. Gli3 coordinates three-dimensional patterning and growth of the tectum and cerebellum by integrating Shh and Fgf8 signaling. Development. 2008; 135:2093–2103. [PubMed: 18480159]

Boehm B, Westerberg H, Lesnicar-Pucko G, Raja S, Rautschka M, Cotterell J, Swoger J, Sharpe J. The role of spatially controlled cell proliferation in limb bud morphogenesis. PLoS Biol. 2010; 8:e1000420. [PubMed: 20644711]

Büscher D, Bosse B, Heymer J, Rüther U. Evidence for genetic control of Sonic hedgehog by Gli3 in mouse limb development. Mech Dev. 1997; 62:175–182. [PubMed: 9152009]

Chen Y, Knezevic V, Ervin V, Hutson R, Ward Y, Mackem S. Direct interaction with Hoxd proteins reverses Gli3-repressor function to promote digit formation downstream of Shh. Development. 2004; 131:2339–2347. [PubMed: 15102708]

Chiang C, Litingtung Y, Harris MP, Simandl BK, Li Y, Beachy PA, Fallon JF. Manifestation of the limb prepattern: limb development in the absence of sonic hedgehog function. Dev Biol. 2001; 236:421–435. [PubMed: 11476582]

Dunn NR, Winnier GE, Hargett LK, Schrick JJ, Fogo AB, Hogan BLM. Haploinsufficient phenotypes in *Bmp4* heterozygous null mice and modification by mutations in *Gli3* and *Alx4*. Dev Biol. 1997; 188:235–247. [PubMed: 9268572]

Galli A, Robay D, Osterwalder M, Bao X, Bénazet JD, Tariq M, Paro R, Mackem S, Zeller R. Distinct roles of Hand2 in initiating polarity and posterior Shh expression during the onset of mouse limb bud development. PLoS Genet. 2010; 6:e1000901. [PubMed: 20386744]

Gerdes J, Schwab U, Lemke H, Stein H. Production of a mouse monoclonal antibody reactive with a human nuclear antigen associated with cell proliferation. Int J Cancer. 1983; 31:13–20. [PubMed: 6339421]

Gros J, Hu JK, Vinegoni C, Feruglio PF, Weissleder R, Tabin CJ. WNT5A/JNK and FGF/MAPK pathways regulate the cellular events shaping the vertebrate limb bud. Curr Biol. 2010; 20:1993–2002. [PubMed: 21055947]

Grossel MJ, Baker GL, Hinds PW. cdk6 can shorten G(1) phase dependent upon the N-terminal INK4 interaction domain. J Biol Chem. 1999; 274:29960–29967. [PubMed: 10514479]

Harfe BD, Scherz PJ, Nissim S, Tian H, McMahon AP, Tabin CJ. Evidence for an expansion-based temporal Shh gradient in specifying vertebrate digit identities. Cell. 2004; 118:517–528. [PubMed: 15315763]

Hill P, Götz K, Rüther U. A SHH-independent regulation of Gli3 is a significant determinant of anteroposterior patterning of the limb bud. Dev Biol. 2009; 328:506–516. [PubMed: 19248778]

Hui CC, Joyner AL. A mouse model of greig cephalopolysyndactyly syndrome: the extra-toesJ mutation contains an intragenic deletion of the Gli3 gene. Nat Genet. 1993; 3:241–246. [PubMed: 8387379]

Jiang J, Hui CC. Hedgehog signaling in development and cancer. Dev Cell. 2008; 15:801–812. [PubMed: 19081070]

Litingtung Y, Dahn RD, Li Y, Fallon JF, Chiang C. Shh and Gli3 are dispensable for limb skeleton formation but regulate digit number and identity. Nature. 2002; 418:979–983. [PubMed: 12198547]

Liu W, Selever J, Wang D, Lu MF, Moses KA, Schwartz RJ, Martin JF. Bmp4 signaling is required for outflow-tract septation and branchial-arch artery remodeling. Proc Natl Acad Sci USA. 2004; 101:4489–4494. [PubMed: 15070745]

Malumbres M, Sotillo R, Santamaría D, Galán J, Cerezo A, Ortega S, Dubus P, Barbacid M. Mammalian cells cycle without the D-type cyclin-dependent kinases Cdk4 and Cdk6. Cell. 2004; 118:493–504. [PubMed: 15315761]

Maynard TM, Jain MD, Balmer CW, LaMantia AS. High-resolution mapping of the Gli3 mutation extra-toes reveals a 51.5-kb deletion. Mamm Genome. 2002; 13:58–61. [PubMed: 11773971]

McGlinn E, van Bueren KL, Fiorenza S, Mo R, Poh AM, Forrest A, Soares MB, de Bonaldo MF, Grimmond S, Hui CC, et al. Pax9 and Jagged1 act downstream of Gli3 in vertebrate limb development. Mech Dev. 2005; 122:1218–1233. [PubMed: 16169709]

Neganova I, Lako M. G1 to S phase cell cycle transition in somatic and embryonic stem cells. J Anat. 2008; 213:30–44. [PubMed: 18638068]

Ng LJ, Wheatley S, Muscat GE, Conway-Campbell J, Bowles J, Wright E, Bell DM, Tam PP, Cheah KS, Koopman P. SOX9 binds DNA, activates transcription, and coexpresses with type II collagen during chondrogenesis in the mouse. Dev Biol. 1997; 183:108–121. [PubMed: 9119111]

Nissim S, Hasso SM, Fallon JF, Tabin CJ. Regulation of Gremlin expression in the posterior limb bud. Dev Biol. 2006; 299:12–21. [PubMed: 16989805]

Ogasawara T, Kawaguchi H, Jinno S, Hoshi K, Itaka K, Takato T, Nakamura K, Okayama H. Bone morphogenetic protein 2-induced osteoblast differentiation requires Smad-mediated down-regulation of Cdk6. Mol Cell Biol. 2004; 24:6560–6568. [PubMed: 15254224]

Ota S, Zhou ZQ, Keene DR, Knoepfler P, Hurlin PJ. Activities of N-Myc in the developing limb link control of skeletal size with digit separation. Development. 2007; 134:1583–1592. [PubMed: 17360777]

Pizette S, Niswander L. BMPs are required at two steps of limb chondrogenesis: formation of prechondrogenic condensations and their differentiation into chondrocytes. Dev Biol. 2000; 219:237–249. [PubMed: 10694419]

Probst S, Kraemer C, Demougin P, Sheth R, Martin GR, Shiratori H, Hamada H, Iber D, Zeller R, Zuniga A. SHH propagates distal limb bud development by enhancing CYP26B1-mediated retinoic acid clearance via AER-FGF signalling. Development. 2011; 138:1913–1923. [PubMed: 21471156]

Riddle RD, Johnson RL, Laufer E, Tabin C. *Sonic hedgehog* mediates the polarizing activity of the ZPA. Cell. 1993; 75:1401–1416. [PubMed: 8269518]

Scherz PJ, Harfe BD, McMahon AP, Tabin CJ. The limb bud Shh-Fgf feedback loop is terminated by expansion of former ZPA cells. Science. 2004; 305:396–399. [PubMed: 15256670]

Schimmang T, Lemaistre M, Vortkamp A, Rüther U. Expression of the zinc finger gene Gli3 is affected in the morphogenetic mouse mutant extra-toes (Xt). Development. 1992; 116:799–804. [PubMed: 1289066]

Scotti M, Kmita M. Recruitment of 5′ Hoxa genes in the allantois is essential for proper extra-embryonic function in placental mammals. Development. 2012; 139:731–739. [PubMed: 22219351]

Sherr CJ, Roberts JM. Inhibitors of mammalian G1 cyclin-dependent kinases. Genes Dev. 1995; 9:1149–1163. [PubMed: 7758941]

Sheth R, Bastida MF, Ros M. Hoxd and Gli3 interactions modulate digit number in the amniote limb. Dev Biol. 2007; 310:430–441. [PubMed: 17714700]

Suzuki T, Hasso SM, Fallon JF. Unique SMAD1/5/8 activity at the phalanx-forming region determines digit identity. Proc Natl Acad Sci USA. 2008; 105:4185–4190. [PubMed: 18334652]

ten Berge D, Brugmann SA, Helms JA, Nusse R. Wnt and FGF signals interact to coordinate growth with cell fate specification during limb development. Development. 2008; 135:3247–3257. [PubMed: 18776145]

te Welscher P, Fernandez-Teran M, Ros MA, Zeller R. Mutual genetic antagonism involving GLI3 and dHAND prepatterns the vertebrate limb bud mesenchyme prior to SHH signaling. Genes Dev. 2002a; 16:421–426. [PubMed: 11850405]

te Welscher P, Zuniga A, Kuijper S, Drenth T, Goedemans HJ, Meijlink F, Zeller R. Progression of vertebrate limb development through SHH-mediated counteraction of GLI3. Science. 2002b; 298:827–830. [PubMed: 12215652]

Towers M, Mahood R, Yin Y, Tickle C. Integration of growth and specification in chick wing digit-patterning. Nature. 2008; 452:882–886. [PubMed: 18354396]

Varjosalo M, Li SP, Taipale J. Divergence of hedgehog signal transduction mechanism between Drosophila and mammals. Dev Cell. 2006; 10:177–186. [PubMed: 16459297]

Verheyden JM, Sun X. An Fgf/Gremlin inhibitory feedback loop triggers termination of limb bud outgrowth. Nature. 2008; 454:638–641. [PubMed: 18594511]

Vokes SA, Ji H, Wong WH, McMahon AP. A genome-scale analysis of the cis-regulatory circuitry underlying sonic hedgehog-mediated patterning of the mammalian limb. Genes Dev. 2008; 22:2651–2663. [PubMed: 18832070]

Wang B, Fallon JF, Beachy PA. Hedgehog-regulated processing of Gli3 produces an anterior/posterior repressor gradient in the developing vertebrate limb. Cell. 2000; 100:423–434. [PubMed: 10693759]

Wang H, Ge G, Uchida Y, Luu B, Ahn S. Gli3 is required for maintenance and fate specification of cortical progenitors. J Neurosci. 2011; 31:6440–6448. [PubMed: 21525285]

Wen X, Lai CK, Evangelista M, Hongo JA, de Sauvage FJ, Scales SJ. Kinetics of hedgehog-dependent full-length Gli3 accumulation in primary cilia and subsequent degradation. Mol Cell Biol. 2010; 30:1910–1922. [PubMed: 20154143]

Witte F, Chan D, Economides AN, Mundlos S, Stricker S. Receptor tyrosine kinase-like orphan receptor 2 (ROR2) and Indian hedgehog regulate digit outgrowth mediated by the phalanx-forming region. Proc Natl Acad Sci USA. 2010; 107:14211–14216. [PubMed: 20660756]

Yoon BS, Ovchinnikov DA, Yoshii I, Mishina Y, Behringer RR, Lyons KM. Bmpr1a and Bmpr1b have overlapping functions and are essential for chondrogenesis in vivo. Proc Natl Acad Sci USA. 2005; 102:5062–5067. [PubMed: 15781876]

Zakany J, Zacchetti G, Duboule D. Interactions between HOXD and Gli3 genes control the limb apical ectodermal ridge via Fgf10. Dev Biol. 2007; 306:883–893. [PubMed: 17467687]

Zeller R, López-Ríos J, Zuniga A. Vertebrate limb bud development: moving towards integrative analysis of organogenesis. Nat Rev Genet. 2009; 10:845–858. [PubMed: 19920852]

Zhu J, Nakamura E, Nguyen MT, Bao X, Akiyama H, Mackem S. Uncoupling Sonic hedgehog control of pattern and expansion of the developing limb bud. Dev Cell. 2008; 14:624–632. [PubMed: 18410737]

Zúñiga A, Zeller R. Gli3 (Xt) and formin (ld) participate in the positioning of the polarising region and control of posterior limb-bud identity. Development. 1999; 126:13–21. [PubMed: 9834182]

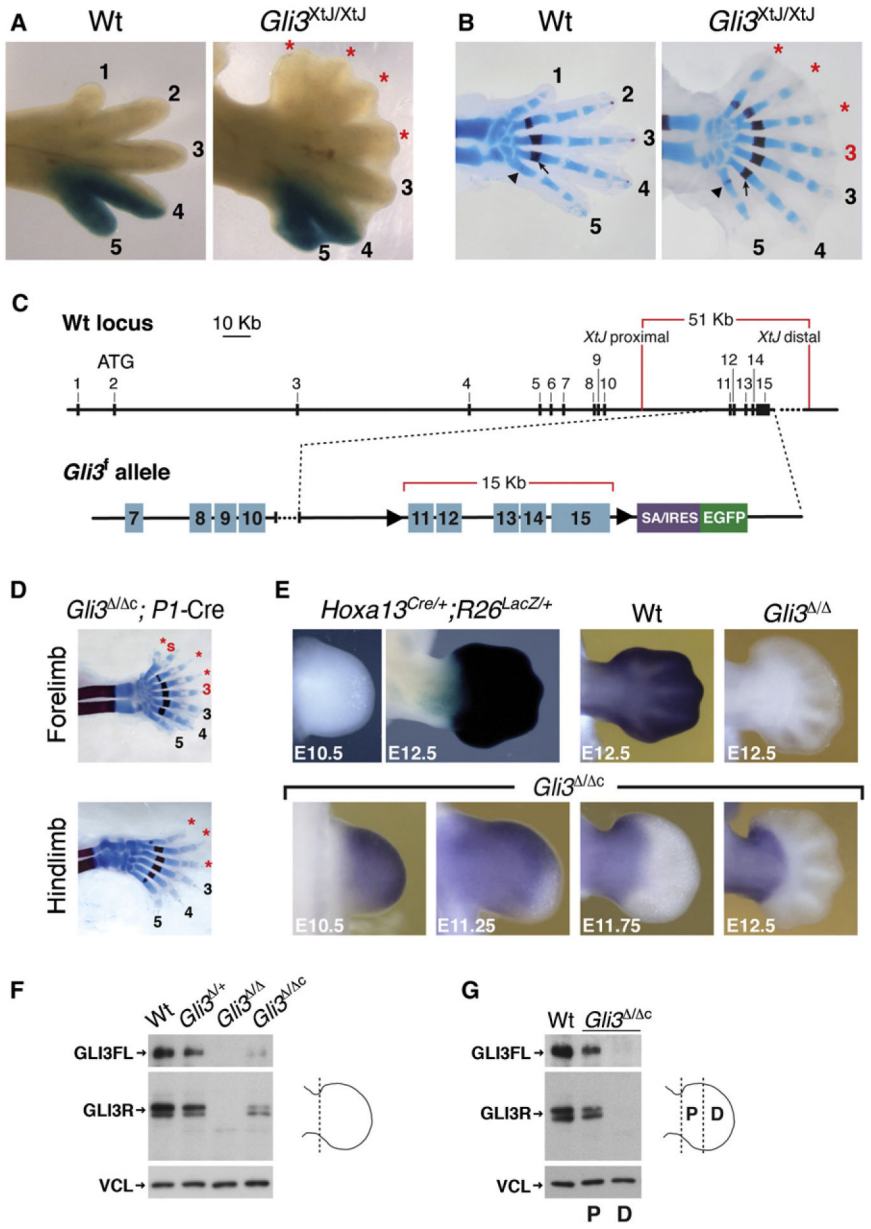

Figure 1. Preaxial Polydactyly and Conditional Inactivation of *Gli3* during Mouse Autopod Development

(A) *Shh*-Cre-mediated activation of a *LacZ* transgene inserted into the mouse *Rosa26* locus was used to map *Shh* descendants in wild-type and *Gli3*-deficient forelimbs. Wild-type (Wt) genotype, $Shh^{Cre/+}$, $R26^{LacZ/+}$; $Gli3^{XtJ/XtJ}$, *Gli3*-deficient embryo carrying the $Shh^{Cre/+}$ and $R26^{LacZ/+}$ alleles.

(B) Forelimb skeletons at E16.5. The mineralization of metacarpal bones (red; cartilage appears blue) in combination with the number and length of phalanges allows identification of posterior digits in wild-type (Wt) and *Gli3*-deficient ($Gli3^{XtJ/XtJ}$) embryos (see also Figure S1).

(C) Scheme depicting the *Gli3* locus and *Gli3* conditional allele. Deletion results in complete loss of function identical to the $Gli3^{XtJ}$ null allele. Black triangles indicate *loxP* sites (see also Figure S1).

(D) Inactivation of *Gli3* in the limb bud mesenchyme from early stages onward using the *Prx1*-Cre transgene (*P1*-Cre) results in fore- and hindlimb polydactylies indistinguishable from $Gli3^{XtJ/XtJ}$ limbs.

(E) Upper left panels show the *Hoxa13*-Cre transgene recombines the $R26^{LacZ/+}$ reporter specifically in the distal part of the forming autopod. Upper right and lower panels illustrate the clearing of *Gli3* transcripts that was assessed by RNA in situ hybridization. Wt and $Gli3^{\Delta/\Delta}$ embryos were used as positive and negative controls (upper right panels). $Hoxa13^{Cre/+}$-mediated recombination of the $Gli3^{f}$ allele produces the $Gli3^{\Delta c}$ allele.

(F) Immunoblot analysis of full-length (GLI3FL) and processed GLI3 repressor (GLI3R) protein in forelimb hand plates at E11.75. Protein extracts were normalized for Vinculin content (VCL).

(G) Immunoblot analysis of GLI3 protein in $Gli3^{\Delta/\Delta c}$ forelimb hand plates dissected into proximal (P) and distal (D) portions.

For digit nomenclatures in (A), (B), (D), and all subsequent figures, normal digits with respect to position and morphology are indicated in black. Duplicated and/or additional digits in *Gli3*-deficient forelimbs are indicated in red. Red asterisks indicate hypomorphic digits or digits with uncertain identity. *s, “split” digit due to duplication of distal phalanges.

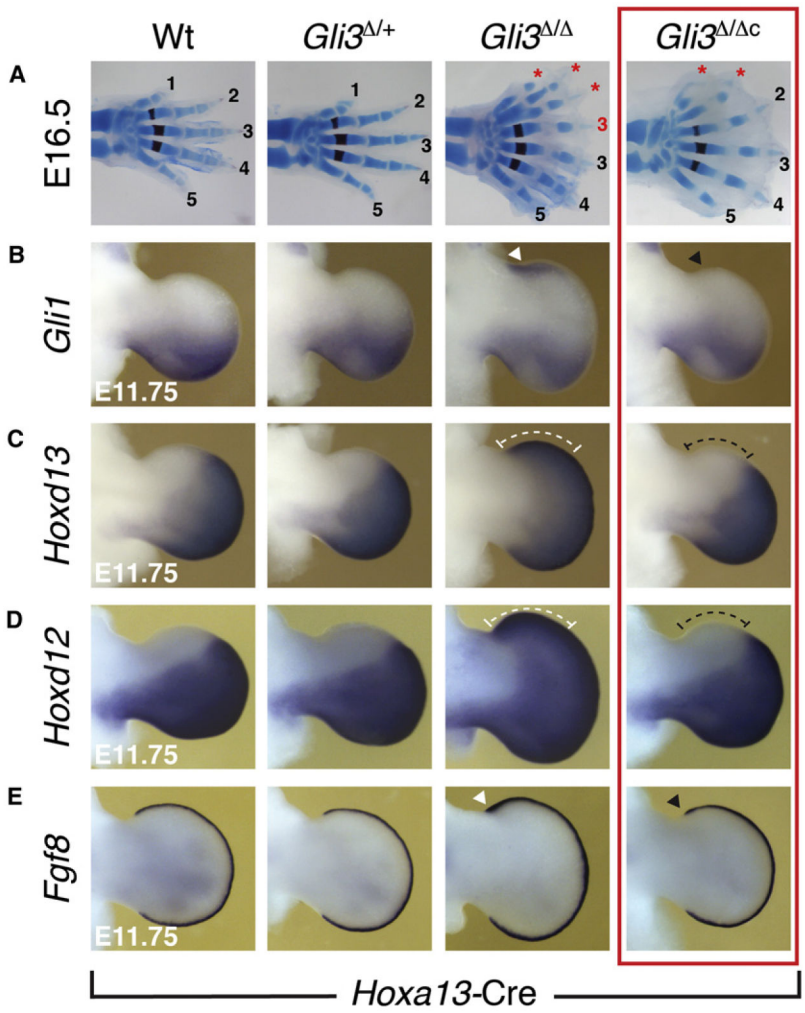

Figure 2. *Hoxa13*-Cre-Mediated Inactivation of *Gli3* Uncouples Preaxial Polydactyly from the Loss of AP Axis Specification

(A) Analysis of forelimb skeletons at E16.5.

(B–E) Analysis of the spatial distribution of *Gli1* (B), *Hoxd13* (C), *Hoxd12* (D), and AER-*Fgf8* transcripts (E) in forelimb buds (E11.75, 50–52 somites). Ectopic (white arrowheads) and normal (black arrowheads) expression domains of *Gli1* and *Fgf8* are indicated. Broken lines mark the expanded (white) and normal (black) expression of *5′ Hoxd* genes in $Gli3^{\Delta/\Delta}$ and $Gli3^{\Delta/\Delta c}$ forelimb buds. All forelimb buds analyzed carried one $Hoxa13^{Cre/+}$ allele to exclude possible phenotypic variation due to heterozygosity for *Hoxa13* (see also Figure S2).

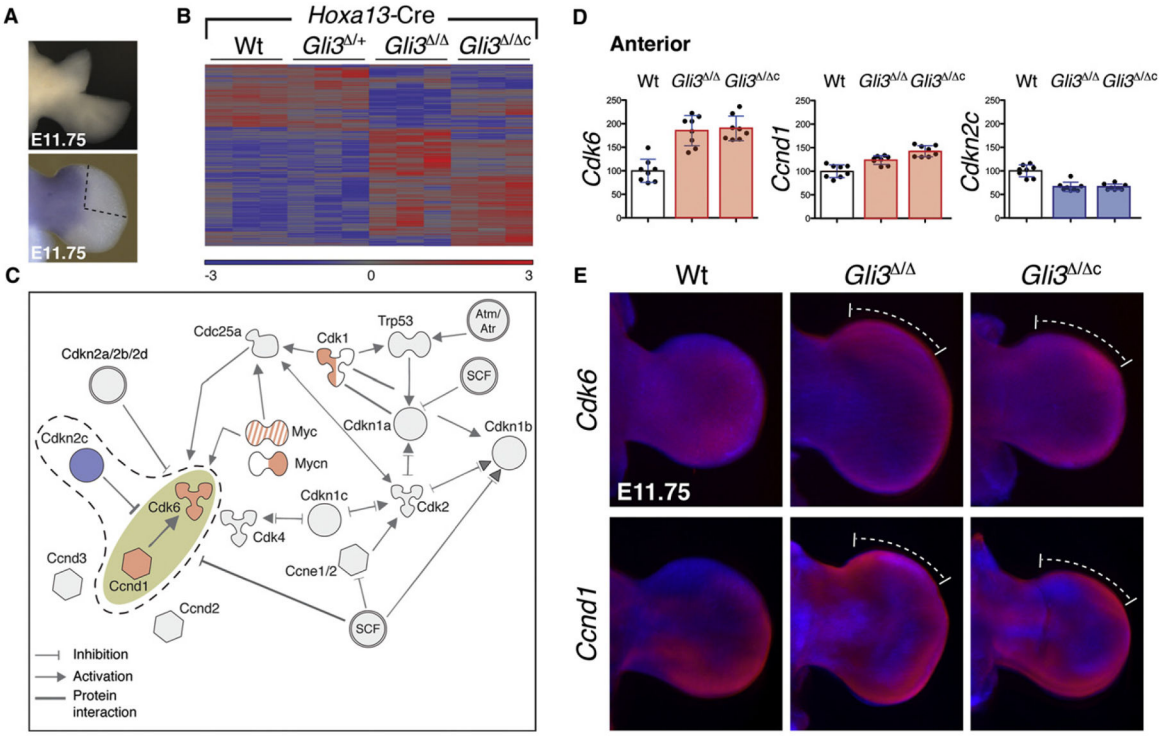

Figure 3. The G_1–S Transition of the Cell Cycle Is Altered in the Anterior Mesenchyme of Both Types of *Gli3*-Deficient Forelimb Buds

(A) Anterior forelimb autopods dissected for transcriptome analysis at E11.75. Lower panel shows the clearance of *Gli3* RNAs from the dissected anterior regions in $Gli3^{\Delta/\Delta c}$ mutants.

(B) Hierarchical clustering of the significant transcriptome alterations ($p \leq 0.05$ in all paired comparisons using two-way ANOVA tests). Red, genes upregulated; blue, genes downregulated.

(C) Ingenuity Pathway Analysis was used to uncover the transcriptional alterations shared by $Gli3^{\Delta/\Delta}$ and $Gli3^{\Delta/\Delta c}$ anterior forelimbs. The core module that regulates the G_1–S transition of the cell cycle is indicated by a broken line. Orange-red labeling of *Ccnd1* and *Cdk6* indicates significantly increased expression. *Cdk1*, *Mycn*, increased expression in only one *Gli3*-deficiency. *Myc*, alteration was not confirmed by qPCR. Blue labeling of *Cdkn2c* indicates significantly decreased expression.

(D) Validation of the alterations in *Cdk6*, *Ccnd1*, and *Cdkn2c* transcript levels by qPCR (n = 8, E11.75, ~52 somites). Statistically significant changes are indicated in blue (downregulation) and orange-red (upregulation). All results are represented as mean ± SD; $p \leq 0.01$.

(E) The spatial distribution of *Cdk6* and *Ccnd1* transcripts was analyzed by RNA in situ hybridization in combination with optical projection tomography (OPT), which results in improved spatial resolution of low and/or widely expressed genes. Limb bud morphology is shown in the blue channel, whereas transcript distribution is shown in the red channel. Broken white lines indicate the anterior domains with expanded expression.

All forelimb buds analyzed were heterozygous for the $Hoxa13^{Cre/+}$ allele.

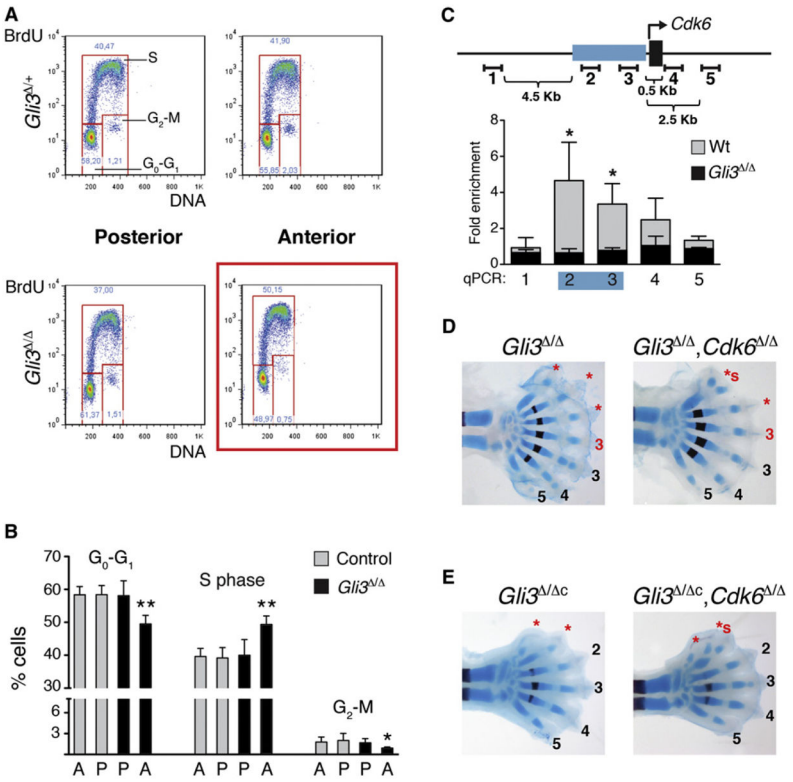

Figure 4. Enhanced S Phase Entry Contributes to the Preaxial Polydactyly in *Gli3*-Deficient Forelimb Buds

(A) Flow cytometric cell-cycle analysis of anterior and posterior limb bud cells in representative control ($Gli3^{\Delta/+}$) and $Gli3^{\Delta/\Delta}$ autopod samples at E11.75. Limb bud cells were gated to define three populations in the G_0–G_1, S, or G_2–M phases of the cell cycle.

(B) Analysis of several $Gli3^{\Delta/\Delta}$ (n = 5) and control (Wt, n = 3; and $Gli3^{\Delta/+}$, n = 4) samples to reveal cell-cycle alterations. Wt and $Gli3^{\Delta/+}$ forelimb autopods were pooled as controls because no significant differences were detected by analyzing individual samples. All data are shown as mean ± SD. **p ≤ 0.01; *p ≤ 0.05. A, anterior limb bud; P, posterior limb bud.

(C) ChIP-qPCR using GLI3 antibodies detects interactions of the endogenous GLI3 proteins with the *Cdk6* locus. The blue region corresponds to a 3 kb fragment identified by Vokes et al. (2008) (mm9: chr5: 3,341,265–3,344,289) that includes the proximal promoter. Amplicons “2” and “3” are located in the critical region. All results are shown as mean ± SD (n ≥ 3; p ≤ 0.05).

(D and E) Skeletal phenotypes resulting from additional inactivation of *Cdk6* in $Gli3^{\Delta/\Delta}$ and $Gli3^{\Delta/\Delta c}$ forelimb buds.

All forelimb buds analyzed carried one $Hoxa13^{Cre/+}$ allele. See also Figure S3.

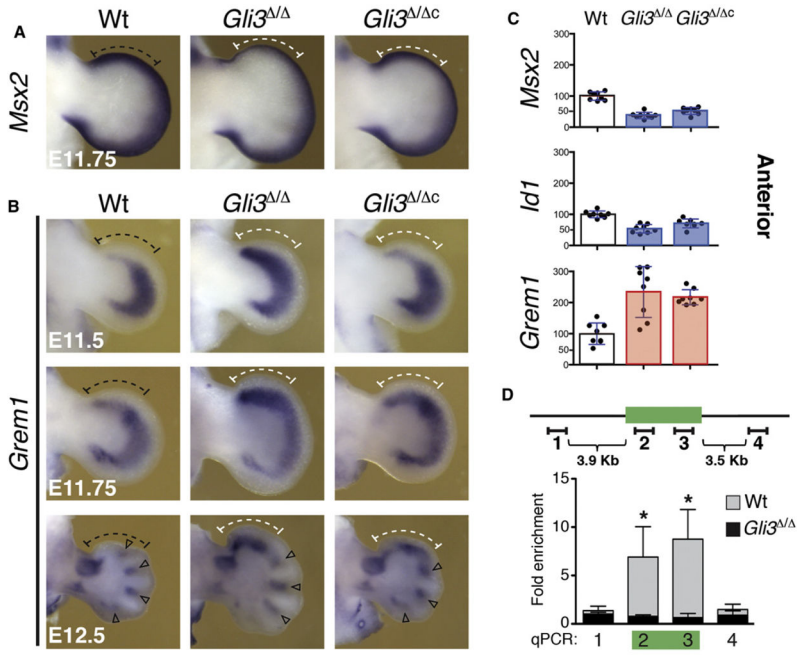

Figure 5. Loss of *Gli3* Decreases BMP Activity in Anterior Forelimb Buds

(A) *Msx2* expression in $Gli3^{\Delta/\Delta}$ and $Gli3^{\Delta/\Delta c}$ forelimb buds (E11.75).

(B) Alterations in the expression of the BMP antagonist *Grem1* in forelimbs. Broken lines indicate the relevant anterior regions in wild-type (black) and *Gli3*-deficient forelimb buds (white). Open arrowheads point to *Grem1* expression in the proximal interdigital mesenchyme, which does not contribute to the digit primordia.

(C) qPCR analysis of two transcriptional BMP targets, *Msx2* and *Id1*, and the BMP antagonist *Grem1* (n = 8, E11.75). Statistically significant changes are indicated in blue (downregulation) and orange-red (upregulation). All results are represented as mean ± SD; $p \leq 0.01$.

(D) ChIP-qPCR using GLI3 antibodies detects interactions of the endogenous GLI3 proteins with a conserved element within the *Grem1-Fmn1* regulatory landscape (indicated in green; Vokes et al., 2008) (mm9: chr2: 113,481,000–113,481,438). Amplicons “2” and “3” are located in the critical region. All results are shown as mean ± SD ($n \geq 3$; $p \leq 0.05$).

All forelimb buds shown were heterozygous for the $Hoxa13^{Cre/+}$ allele. See also Figure S4.

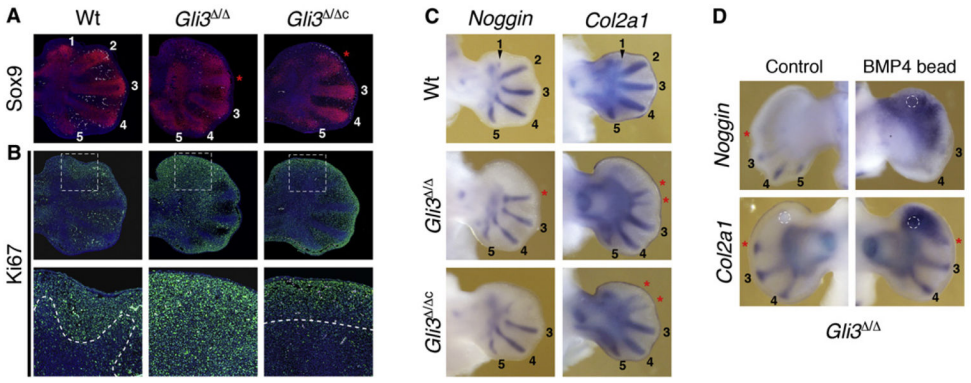

Figure 6. The Exit of Proliferating Progenitors to Chondrogenesis Is Delayed in the Anterior of *Gli3*-Deficient Autopods

(A) Sox9 (red fluorescence) demarcates the forming digit primordia on sections of wild-type, *Gli3*$^{\Delta/\Delta}$, and *Gli3*$^{\Delta/\Delta c}$ autopods (E12.5, ~60 somites).

(B) The Ki67 antigen (green fluorescence) marks proliferating cells, whereas the autofluorescent erythrocytes appear white. Cell nuclei appear blue due to counterstaining with Hoechst-33258. In the upper panels, dotted rectangles indicate the position of the enlargements. In the left and right lower panels, dotted white lines indicate the proximal limit of the mesenchymal zone with largely Ki67-positive cells.

(C) *Noggin* and *Col2a1* transcripts mark the ongoing chondrogenesis during digit formation at E12.5.

(D) RNA in situ hybridization revealed the induction of *Noggin* (n = 13/16) and *Col2a1* (n = 10/13) expression (right panels) following implantation of BMP4-loaded beads (0.5 mg/ml) into the anterior of *Gli3*$^{\Delta/\Delta}$ forelimb buds at E12.0. Contralateral controls with no or PBS-soaked beads (left panels).

All relevant forelimb buds in (A)–(C) carried one *Hoxa13*$^{Cre/+}$ allele.

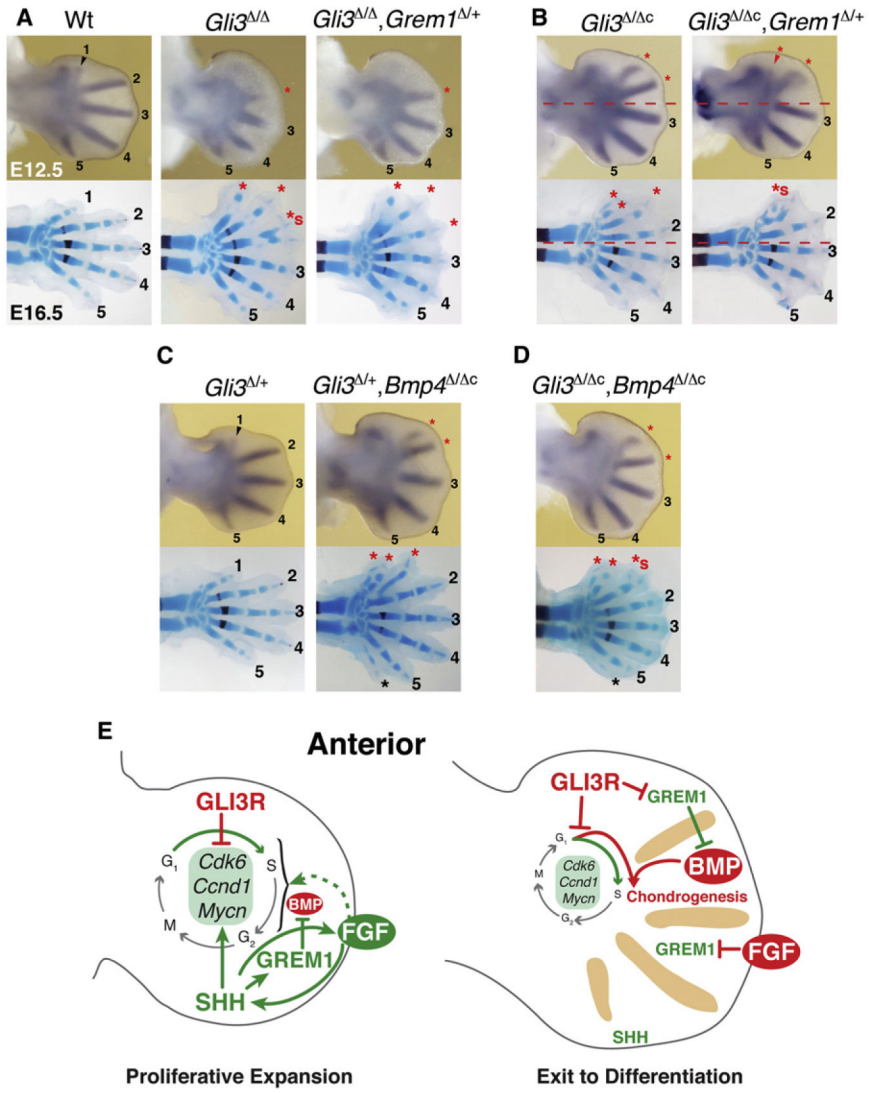

Figure 7. Reduction and Promotion of Preaxial Polydactyly by Altering *Grem1*, *Bmp4*, and *Gli3* Gene Dose

Comparative analysis of genetic alteration of BMP pathway activity in the context of both types of *Gli3* deficiencies. *Col2a1* expression at E12.5 detects mesenchymal condensations (upper panels), which is compared with the resulting skeletal pattern at E16.5 (lower panels). In the upper panels, arrowheads indicate the small condensation for digit 1; red asterisks point to reduced or forked digit primordia with uncertain identity. In the lower panels, black asterisks indicate postaxial condensations. Figure S5 shows the skeletal preparations of all genotypes analyzed.

(A) Wild-type (i.e., $Hoxa13^{Cre/+}$) forelimbs compared to $Gli3^{\Delta/\Delta}$ (n = 6) and $Gli3^{\Delta/\Delta}$, $Grem1^{\Delta/+}$ forelimbs (n = 9).

(B) Constitutive genetic inactivation of one *Grem1* allele in $Gli3^{\Delta/\Delta c}$ forelimb buds.

(C) $Gli3^{\Delta/+}$forelimb buds carrying the $Hoxa13^{Cre/+}$ allele compared with $Gli3^{\Delta/+}$, $Bmp4^{\Delta/\Delta c}$ forelimbs in which one *Bmp4* allele was conditionally inactivated by *Hoxa13*-Cre.

(D) $Gli3^{\Delta/\Delta c}$, $Bmp4^{\Delta/\Delta c}$ forelimb buds.

(E) Regulation of the proliferative expansion and chondrogenic exit of digit progenitors by GLI3R and SHH-dependent gene networks. Green indicates genetic interactions positively regulating proliferation; red shows genetic interactions restraining the cell cycle and promoting exit to chondrogenic differentiation.